Mobility and solvation of ions in channels

R. M. Lynden-Bell
Atomistic Simulation Group, School of Mathematics and Physics, The Queen's University, Belfast BT7 1NN, United Kingdom

Jayendran C. Rasaiah
Department of Chemistry, University of Maine, Orono, Maine 04469

(Received 28 May 1996; accepted 22 August 1996)

In this paper we present some results from a simulation study of the mobility and solvation of ions and uncharged molecules in aqueous solution in smooth cylindrical channels at room temperature. This ideal system provides a reference system with which to compare the behavior of water and ions in real porous materials such as zeolites, bucky tubes, and biological channels. We find that in channels of radii between 2.5 and 5.5 Å the water molecules form a cylindrical solvation shell inside the channel walls with some evidence of a second shell in the center of the largest channel. Not all protons are involved in hydrogen bonding and a number point toward the walls. We attribute this to the concavity of the surface. When a sodium ion is added it tends to lie in the center of the channel where it can form the most complete solvation shell. Its diffusion rate decreases in smaller channels until it moves too slowly in a channel of 2 Å radius to be detected in our simulations. This decrease is only partly due to an increase in the mean square force on the ion. A range of ions of different sizes were studied in a channel with radius 3 Å. While the smaller of these ions (F^-, Na^+, and Ca^{++}) lie preferentially in the center of the channel, larger ions (Cl^-, I^-, and Cs^+) penetrate some way into the layer of water inside the wall and methane and ions with the charges turned off move next to the wall. Landau free energy analysis shows that this change is due to the balance between entropy and energy. The behavior in smooth channels is quite the opposite of what has been observed in experimental studies and simulations of Gramicidin (pore radius of 2 Å), where Cs^+ lies closer to the center of the channel and Na^+ lies off the axis. This difference can be attributed to the specific molecular structure of the gramicidin pores (e.g., the presence of carbonyl groups). As in bulk solutions, the mobilities of the ions in smooth channels increase to a maximum with ion size and decrease with increasing magnitude of the charge on the ion, while uncharged species diffuse much more rapidly and show a monotonic decrease with size. This behavior is related to the characteristics of the fluctuations of the forces on the solute molecules. [S0021-9606(96)50944-X]

I. INTRODUCTION

The mobility of water and hydrated ions in channels or micropores is important in biological systems (e.g., ion channels in membranes) and in many systems of interest to chemistry and chemical engineering (e.g., porous materials including zeolites and bucky tubes). Selectivity of specific ions (e.g., the potassium ion) and a high rate of transport are distinctive features of these pores but are incompletely understood. Some aspects of biological channels are quite intriguing. For instance, the amino acid sequences of several biological channels have been deduced and it has been observed that the mutation of a single amino acid residue in one case can transform a sodium ion channel to a channel permeable to calcium ions, while the substitution of three amino acids in another is able to convert a cation selective channel to an anion selective pore.[1,2] The key questions are: How are the selectivity and mobility of ions affected by the pore and ion sizes, the ion charge and the structure, and the charge distribution and conformational changes of the channel membrane? Some of these problems have been addressed in experimental and theoretical studies and by modeling, but our understanding is still rudimentary.[3–16]

Computer simulation has been used for many years to study the behavior of molecules in porous media.[17] Much of this work has been with slit-shaped pores and zeolites, but Murad *et al.*[18] have looked at Lennard-Jones fluids in model pores of different shapes and Peterson *et al.*[19] have studied the same fluids in cylindrical channels. Suh *et al.*[20] have studied the diffusion of hard sphere fluids in hard cylinders and recently Sansom *et al.*[21] have looked at the structure and dynamics of water in channels that are similar to those studied here. A great deal of effort has also been put into more realistic modeling of biological channels, particularly gramicidin, by McKay *et al.*,[12] Jordan,[4–7] Chiu *et al.*,[14,15] Aquist and Warshel,[16] Roux and Karplus,[1,2] and others.[8,22] Most of the studies of biological channels attempt to include the specific structure of the channel concerned, which makes their analysis quite complicated.

Our aim in the work described in this paper is to study a very simple model as a reference system for the behavior of water and aqueous solutions in pores. We use this to try to isolate some of the factors involved in the transport of water and ions through micropores in general rather than to study a particular system. By comparison with real pores and bulk fluids, we also hope to learn more about the mechanism of

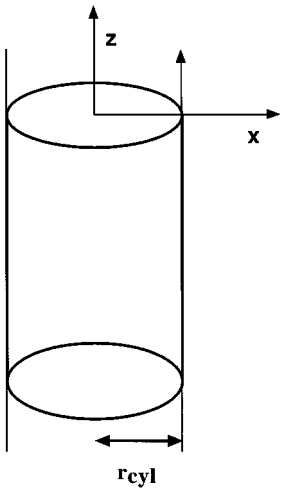

FIG. 1. Cylindrical simulation cell for molecular dynamics study of ion mobility and solvation in smooth channels. Periodic boundary conditions apply only in the z direction which is along the axis of the cylinder.

ion transport in confined systems of biological and chemical significance. For instance, our simulations of simple cations in smooth channels lead to results, for pores larger than 3 Å in radius, that are similar to their transport in bulk fluids but are rather different from what is known about their behavior is gramicidin (pore radius of 2 Å), which is blocked by the divalent cation Ca^{2+} and is essentially impermeable to Cl^- ions.

Our model comprises an infinite cylindrical pore with smooth walls containing water molecules and ions of various types. In addition to studying common ions such as Na^+, Ca^{2+}, Cl^-, and others we have taken advantage of the simulation method to change the characteristics of the ion (e.g., by switching off or reversing the sign of the charge) in order to try to understand the causes of the behavior we see. In particular, switching off the charges changes a solute from being hydrophilic to hydrophobic and we interpret some of the changes in behavior in terms of entropic and energetic effects.

II. COMPUTATIONAL DETAILS

Each sample comprises a specified number of water molecules and either a single or no solute molecule in a cylindrical channel with smooth repulsive walls. Figure 1 shows the channel geometry. Periodic boundary conditions are applied in the z direction (which is parallel to the axis of the channel).

The water molecules are rigid entities modeled by the SPC/E potential[23] which has charges of $-0.8476e$ on the O atom and $0.4238e$ on the H atom and a Lennard-Jones center on the O atom. The molecules used as solutes are first a series of real ions, second, hypothetical ions with altered charges, and third, neutral solutes modeled as Lennard-Jones spheres with parameters identical to some of the real ions. The interactions of the ions with the water molecules are also due to charges and Lennard-Jones potentials. Table I summarizes the parameters used. These are taken from the work of Dang *et al.*[24–29] and are the same as used by Lee and Rasaiah in their work on ion mobility in bulk SPC/E water.[30] We used the minimum image convention with a cutoff at 9 Å. We did not apply any long-range corrections. This makes the results comparable to those of Lee and Rasaiah for bulk systems.[30] It is also unclear what long-range corrections would be most appropriate. In a biological membrane pores are about 12 Å long and connect two aqueous environments with a high dielectric constant while the material of the membrane has a much lower permittivity. In inorganic media the pores may be much longer. We do not expect that including some type of long-range correction would affect the comparative ion mobilities or the local structure.

TABLE I. Potential parameters used.

Ion	σ_{iO}/Å	ϵ_{iO}/kJ mol^{-1}	q/e
Na^+	2.876	0.5216	+1
K^+	3.250	0.5216	+1
Cs^+	3.526	0.5216	+1
Ca^{2+}	3.019	0.5216	+2
F^-	3.143	0.6993	−1
Cl^-	3.785	0.5216	+1
I^-	4.168	0.5216	+1
$O(H_2O)$	3.169	0.6502	−0.8476
$H(H_2O)$		0.0	+0.4238

The wall potential was chosen to be steeply repulsive and not to penetrate far into the center of the cylinder. The form used was

$$V_{\text{wall}} = A \exp[-B(r_{\text{cyl}} - R)], \tag{1}$$

where R is the distance of the oxygen atom in the water molecule or the ion from the axis of the cylinder. For these calculations the values chosen were $A = 162$ kJ mol^{-1} and $B = 4.18$ Å^{-1} and the potential was cut off at 2.5 Å from the wall. The same parameters were used for water and all ions. This value of B was chosen to be the same as that used successfully for the O–O repulsion parameters in a number of calculations of salts containing nitrites, nitrates, sulfates, and perrhenates.[31] The value of A was chosen such that the potential energy was equal to kT at 1 Å from the cylinder surface.

At first sight the cylinder wall appears to be extremely hydrophobic. It must be recalled, however, that the interior of a cylindrically symmetric charge distribution has no radial field. This can be understood from a simple physical argument. By symmetry, any components of the field in planes perpendicular to the axis of symmetry must be radial. Radial lines of force could only exist if there were charge density on the cylinder axis to provide a source for them, but there is no axial charge density in a hollow tube such as the ones studied here. If the surface charge distribution is nonuniform along the axial direction (as in a funnel-shaped charge distribution) there may be axial fields but no radial fields. In our cylindrical model pore there would be no electrostatic field even if the wall contained a uniform charge or radial dipole distribution. The effect of such a hydrophilic surface would be to

change the electrostatic potential uniformly throughout the channel. This affects the chemical potential of the ions but not the water, thereby influencing the entrance of an ion to the channel but not its subsequent motion.

There is a problem in choosing the most suitable channel length for a given radius and number of water molecules. Ideally one would like to be able to set the chemical potential of the water to be the same as in some specified bulk solution. This would involve a lengthy series of computations. An alternative is to choose the same density as bulk water. Unfortunately it is difficult to define the density in the channels for two reasons. First, because the wall repulsion is exponential, the radius is not well defined; changing the value of A is equivalent to changing the value of $r_{\rm cyl}$. In all the references to $r_{\rm cyl}$ in this paper it is assumed that a standard value $A=162$ kJ mol^{-1} is used. The second problem is that the water density is highly nonuniform, with the molecules forming a solvation layer inside the surface of the cylinder. We chose a length of the channel l for each radius which gave the same number density of molecules inside the volume $V=l\pi r_{\rm cyl}^2$ as in bulk water.

Even with a given density there is a question as to the effect of the periodic boundary conditions. If the channel length l is too short, correlations of the density and dipoles may be propagated along the channel artificially. The original channel lengths were chosen to contain at least 20 water molecules and, for wider channels a length of about 20 Å. Some runs were carried out for channels of twice the length. In simulations with a solute, one water molecule was replaced by a solute molecule without making any changes in the box size. The imposition of periodic boundary conditions has a greater effect when an ion is present as the axial orientation of water dipoles is propagated further. We are not dealing with infinitely dilute solutions of ions, but with channels of one ion per unit box length. Again we have performed a few runs for more dilute solutions. In particular, all our simulations of single ions in channels of radii of 3 Å and 20 Å long were repeated for channels with twice this length.

The molecular dynamics (MD) program was adapted from that used by Lee and Rasaiah. It uses a fifth-order Gear algorithm and quaternions to describe the motion of the water molecules.[32] The time step was 1 fs except for the simulations with small hypothetical negative ions where it proved necessary to halve the time step. Each run was started from a previous configuration or from a portion of a sample of bulk water. The velocities were chosen randomly from a Gaussian distribution at the required temperature. The sample was allowed to equilibrate for at least 50 ps and data were collected for 1–5 ns. This may seem a long time, but with only one ion such long runs were found to be necessary in order to obtain reproducible results for the diffusion constants. Reliable static averages could be obtained from shorter runs (500 ps). The quantities measured during the run included the potential energy, the ion–water potential energy, the interaction energy with the wall, and the pressure in both the z and in the radial directions. The separate contributions to the energy and the distribution functions for the ion and the oxygen and protons of the water molecule were accumulated as a function of R. Ion positions and velocities and in some cases water positions were stored at intervals for subsequent analysis. All the runs here were carried out at a temperature of 298 K. This was achieved by using Gaussian thermostats which constrained the translational and rotational kinetic energies to be constant[32] together with a weak Berendsen thermostat to overcome drift.

In an anisotropic system, such as that studied in this work, the pressure is a tensor. In our system there are two distinct values, the radial and axial components, which were calculated separately. The axial component, (P_{zz}), was calculated in the usual way from the virial

$$P_{zz}=\left[(N-2)kT+\sum_{ij}F_{z,ij}z_{ij}\right]\Big/V, \tag{2}$$

where the sum is over all pairs ij of the z component of the force on i due to j multiplied by the difference in z coordinates. The factor $(N-2)$ is used because there are two degrees of freedom which are fixed, namely the z components of momentum and angular momentum. The volume V was taken to be equal to

$$V=\pi r_{\rm cyl}^2 l. \tag{3}$$

The radial pressure was measured both by the force per unit area on the surface of the cylinder (assumed to have radius $r_{\rm cyl}$) and by the virial expression

$$P_{\rm rad}=\left[2NkT+\sum_{ij}F_{x,ij}x_{ij}+\sum_{ij}F_{y,ij}y_{ij}+\sum_{i}F_{{\rm wall},i}(r{\rm cyl}-R_i)\right]\Big/2V, \tag{4}$$

where $F_{{\rm wall},i}$ is the force on the ith molecule due to the wall and R_i is its distance from the axis of the cylinder. The results from these two methods agreed within 0.5 MPa (5 bar) or better.

If the liquid in the pore were structureless one could relate these pressures to the surface tension, s, and the internal pressure $P_{\rm int}$. Considering the work done by a cylinder of liquid in expanding its radius from R to $R+dR$ gives

$$P_{\rm rad}A_c dR=P_{\rm int}A_c dR-s dA_c, \tag{5}$$

where $A_c=2\pi Rl$ is the area of the surface of the cylinder in the molecular dynamics box with periodic boundaries at intervals of l. The change in surface area $dA_c=2\pi l dR$. On the other hand the work done in increasing the length of the periodic box by dl is

$$P_{zz}A_x dl=P_{\rm int}A_x dl-s dA_x, \tag{6}$$

where $A_x=\pi R^2$ is the area of the cross section of the cylinder and $dA_x=2\pi R dl$. Combining these two equations we obtain

$$s=R(P_{\rm rad}-P_{zz}),$$
$$P_{\rm int}=2P_{\rm rad}-P_{zz}. \tag{7}$$

Although it is not clear that we can assume that our system has a uniform internal pressure or that the surface of tension

is at the surface of the cylinder, we use these equations with $R=r_{\mathrm{cyl}}$ to evaluate the two quantities s and P_{int} from the two pressure measurements.

A useful relation, which can be derived from the above equations by considering the work done when the radius is increased at constant volume, is the rate of change of free energy per unit cylinder length, A, with cylinder radius, R, at constant density:

$$\left(\frac{\partial A}{\partial R}\right)_{\rho} = +2\pi s. \tag{8}$$

For a structureless solvent, s is constant so that A decreases linearly with R as conditions within the channel become nearer those in the bulk.

The structural information obtained was of two types; first the distribution of ions and molecules relative to the channel, and second the distribution of water molecules relative to the ions. As the channels are cylindrically symmetrical the probability distribution function for any particular type of atom only depends on the perpendicular distance R from the axis of the channel. We measured $p(R)$ for O, H, and solute atoms by constructing histograms of the instantaneous positions. From these the radial densities

$$\rho(R)=(2\pi R)^{-1}p(R) \tag{9}$$

were also calculated. The local environment of each solute was measured in a similar way by constructing the function $n_{\mathrm{SO}}(r)$ (the probability density of finding an O atom at distance r from the solute molecule S) from a histogram of OS distances. Similar functions $n_{\mathrm{OO}}(r)$ and $n_{\mathrm{OH}}(r)$ were calculated for oxygen–oxygen and oxygen–hydrogen, respectively. Coordination numbers were determined by integrating these functions to their first minimum. The mean number of close OH pairs and of hydrogen-bonds per molecule was calculated in the pure water samples. A hydrogen bond was defined when $r_{\mathrm{OH}}\leqslant 2.5$ and the angle OHO was greater than 130°, while a close OH pair was defined as one which satisfied the first criterion, but not necessarily the second.

Various aspects of the dynamics of the samples were explored. In particular the mean square displacements in both the z direction (along the axis) and in the perpendicular direction were determined as a function of time. Multiple time origins separated by 0.8 ps were used for this analysis and the mean square displacements were followed for 50–100 ps. From these quantities the diffusion constants of solute and water molecules along the cylinder axis can be determined by

$$D_{zz}=0.5\left(\frac{d\langle[z(t)-z(0)]^2\rangle}{dt}\right)_{\mathrm{lim}}, \tag{10}$$

where the gradient is taken in the limiting linear region. The diffusion constant is related to the velocity autocorrelation time from

$$D_{zz}=0.5\langle v_z^2\rangle\tau_v, \tag{11}$$

where τ_v is the correlation time for the decay of the normalized velocity autocorrelation function in the z direction (along the cylindrical axis). This equation is exact, although the diffusion constant is only defined for times that are long enough for complete decay of the correlations in the velocities. In the Langevin theory of Brownian motion[33] the diffusion constant can also be related to the behavior of the fluctuations in the forces by

$$D_{zz}=(kT)^2/(\langle F_z^2\rangle\tau_F), \tag{12}$$

where τ_F is the correlation time of the random force F_z. The assumptions of the Langevin theory are that the force correlations decay much more rapidly than the velocity correlations. If this were true then the velocity correlations would decay exponentially. In aqueous solutions of ions the time scales of the decay of force and velocity fluctuations are similar and the velocity correlations certainly do not decay exponentially. Nevertheless, the quantity

$$\gamma=D_{zz}\langle F_z^2\rangle/(kT)^2, \tag{13}$$

which would be equal to τ_F^{-1} in the Langevin limit can be calculated from the measured values of D and $\langle F_z^2\rangle$. This rate, γ, relates in some way to time scales of forces and network fluctuations and gives some insight into the variation of the mobility of the solute molecules.

The Landau free energy is the free energy of a system in which one variable (often known as an order parameter) is constrained. A familiar example of a Landau free energy is the potential of mean force which is the free energy of a system with the separation between two particles constrained to be at some distance r apart. In that case r is the order parameter and we can deduce properties of the system by considering the potential of mean force as a function of r. The most probable values of the order parameter in an unconstrained system correspond to minima in the Landau function. Here we determined the Landau free energy as a function of the radial displacement R of the ion or solute from the axis of the cylinder. The basic relation is

$$A(R)=-kT\,\log[p(R)]+A, \tag{14}$$

where $p(R)dR$ is the probability of finding the ion between R and $R+dR$ and A is the Helmholtz free energy. Using this equation we can determine $A(R)$ (within a constant) by forming a histogram of probabilities. In order to access values of R which have a low intrinsic probability one may add a biasing potential acting on the solute, but not on the water molecules. In this case

$$A(R)=-kT\,\log[P_X(R)]-E_X(R)+A_X, \tag{15}$$

where $p_X(R)$ is the probability distribution observed in the presence of the biasing potential $E_X(R)$ and A_X is a constant whose value depends on the biasing potential. By choosing a number of different functions of $E_X(R)$ one may explore the whole range of values of R and by overlapping the functions $A(R)$ in the different windows determine it over the whole range. Overlapping is important as the constants A_X cannot be determined in this method. This method is closely related to the method of umbrella sampling[32,34] and has been applied recently to melting and freezing in bulk liquids and clusters.[35–37]

Normally these methods are used in Monte Carlo programs, but we used our molecular dynamics program by including an additional radial force $-dE_X(R)/dR$ due to the biasing potential. Two forms of $E_X(R)$ were used. In the first the preexponential term in the solvent-wall potential [Eq. (1)] was varied and in the second a quadratic term in $(R-R_{\mathrm{ref}})$ was added. The water–water, water–ion, and water–wall energy were all binned as a function of R so that the Landau entropy could be found by subtraction using

$$-TS(R)=A(R)-U_{\mathrm{SW}}(R)-U_{\mathrm{WW}}(R)-U_{\mathrm{W\ wall}}(R), \tag{16}$$

where the subscripts W and S refer to water and solute, respectively.

There are two types of errors and uncertainties in the measured values of thermodynamic and dynamic quantities. The first is the accuracy to which one can determine the quantity concerned for the system investigated and the second is the sensitivity of the values to small changes in the system, e.g., the density or channel length. Estimates of the former are shown as error bars or discussed in the figure captions. We have less information about the latter, but comments are made in the text at appropriate places.

III. PURE WATER IN CYLINDRICAL PORES

A. Structure and hydrogen bonding

From the runs with water alone one can examine the effects of confinement on the water structure and the hydrogen-bond network. It is well known that solvation layers are found in water and other liquids near flat walls[38] and solvation shells are seen around spherical and nonspherical solutes.[39] This effect is due to packing. A similar effect is apparent in these cylinders. Figure 2 shows the density distribution of the O and H atoms in the runs with pure water in cylinders of different radii. Looking first at the O atom distribution and remembering that the O atoms are very close to the center of mass of the molecule, we see that in all the cylinders the water molecules form a solvation layer within the wall with a maximum just over 1 Å from the wall. In the channels of radius of 4.5 Å and above there is room for another solvation shell in the channel and a second maximum in the probability density is seen in the center of the channel. This central core of oxygen atoms is particularly apparent in the 4.5 Å radius channel.

There is a contribution to the free energy of the system which depends on whether the cylinder size is commensurate with the natural separation of the solvation layers. This is similar to the effects found in a liquid between a flat surface and a tip or between two flat surfaces where the derivative of the free energy with respect to tip–flat or flat–flat separation gives a solvation force which can be probed in atomic force microscope and similar experiments.[39–41] It was noted in Sec. II that the surface tension s gives a direct measure of the derivative of free energy with respect to channel radius at constant density and that in a continuum solvent model s would be constant. Thus the effects of solvation structure are reflected in the variation of s from a constant value. If the solvation layer structure is commensurate with the channel radius then the free energy relative to a continuum solvent model will be a minimum and will rise to a maximum between the points with n and $n+1$ commensurate solvation shells. The surface tension, which is the derivative of the free energy, will be greater than the continuum value between the points of maximum and minimum stability of the n layer solvent structure and less than the continuum value at radii higher than the maximum stability of n layers and lower than that of $n+1$ layers.

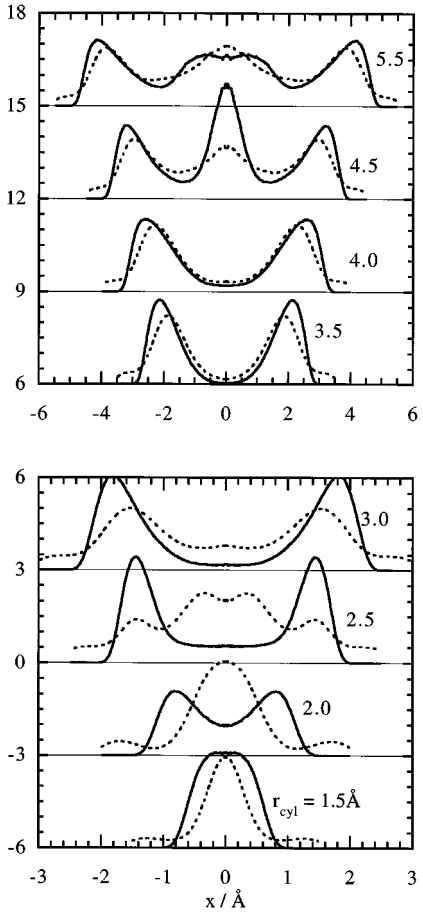

FIG. 2. Density profiles of water across channels of different radii. The solid lines represent the density of oxygen atoms and the dotted lines the hydrogen density. Each graph is marked with the value of the cylinder radius. Note that there is a change of horizontal scale between the upper four and the lower four sets of curves.

Figure 3 shows that most of the cylinders have approximately the same surface tension but the 2 and 4 Å cylinders have lower values. These results suggest that the most stable arrangement with a single water layer inside the cylinder occurs at a slightly larger radius than 4 Å. However when the channel radius is increased to 4.5 Å another solvation layer has appeared. Looking at other data we see that the 4 Å cylinder is anomalous in other ways. It has anomalously low values for the internal pressure (Fig. 3) and for the diffusion constant (Fig. 4). Compared with the trend it has a slightly lower potential energy and there are slightly more ''close hydrogens''—that is, OH pairs separated by less than 2.5 Å.

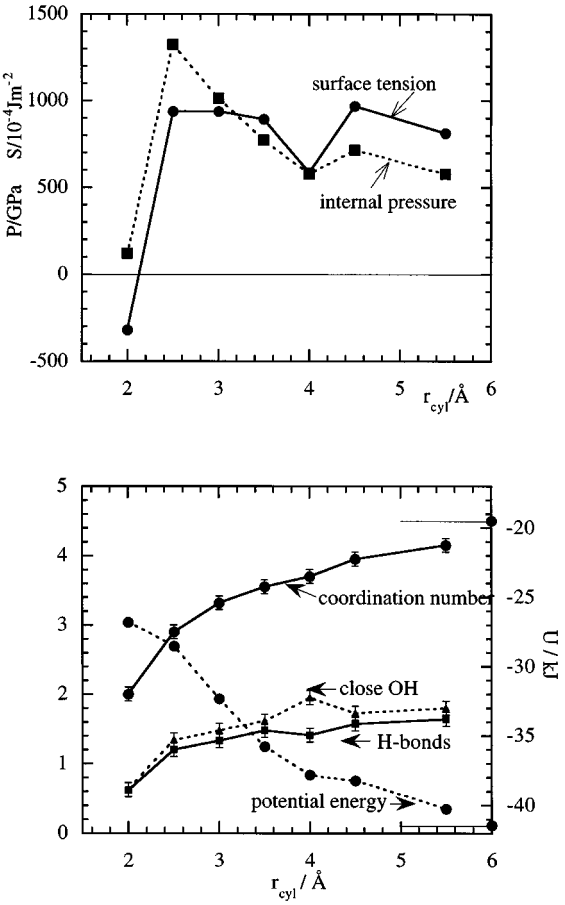

FIG. 3. Structural properties of water as a function of cylinder radius. Upper graph: Surface tension (the full line; units of 10^{-4} J m^{-2}) and internal pressure of water (the dashed line: units of MPa) In both cases the accuracy is 2% or better. Lower graph: Potential energy (right-hand scale) and solvation number, number of hydrogen bonds and close O–H pairs (the left-hand scale). The surface tension and internal pressure were calculated as described in the text. The numbers describe the surroundings of an average molecule, i.e., in the ideal ice structure the solvation number and numbers of hydrogen bonds and close OH pairs would each be equal to 4. The short horizontal lines show the limiting values of the solvation number and potential energy in the bulk.

We deduce that the water structure in the 4 Å cylinder is anomalously stable.

At the molecular level the structure of water is determined by the hydrogen-bonding network. This is affected by the concave surface of the cylinder. In a bulk sample of water nearly all the protons are involved with H bonds. If a small hydrophobic solute is dissolved in water the local hydrogen bond network may be strengthened as the water forms clathratelike structures around the solute.[42,43] Studies of solvation of spheres of various sizes[42–45] show that as the curvature of the sphere decreases the hydrogen-bond network is weakened until adjacent to a flat surface it is no longer possible for every proton to be involved in hydrogen bonds. This trend is continued in our cylinders where the surface is concave. One way in which this can be seen is in the distribution functions for the protons (Fig. 2: dotted lines) which extend nearer to the wall than those for the oxygen atoms (Fig. 2: solid lines); these protons cannot be involved in H bonding. The molecular orientation also varies with radius. The mean dipole in the radial direction is always small and changes sign as the solvation peak is traversed. This suggests that the dipoles preferentially lie perpendicular to the radius vector, and this is confirmed by looking at the orientational quadrupoles, which show that there also is a slight preference for the dipoles to lie in the axial rather than the tangential direction. The number of hydrogen bonds around each water molecule would be equal to four in an ideal ice configuration. It is considerably less than this in all the cylinders, emphasizing the amount the hydrogen-bond network is disrupted by confinement within the concave surfaces of the cylinders. As expected the number of water molecules in the first shell is as low as two in the narrowest cylinders and increases steadily as the width increases.

Another piece of evidence relating to the hydrogen-bond network is the coordination number of the water molecules, which we determined by integrating the average numbers found either to the first minimum in the probability function $n_{OO}(r)$ or to $r=3.5$ Å. The values (shown in Fig. 3) vary from 2 in the narrowest channel where the water molecules are in single file to 4.1 in the broadest channel; all these are less than the value of 4.5 found in bulk water at this temperature. There is a corresponding decrease in the average water potential energy, but no observable change in the position of the first maximum in n_{OO}.

Although the ensemble average of the dipole moment in the axial direction must be zero there is the possibility of instantaneous correlated fluctuations of water molecules in the axial direction. Any correlations on a length scale greater than the periodically repeated unit would be suppressed by the imposition of periodic boundary conditions. We examined the density and axial dipole correlation functions $g(z)$ and $C_\mu(z)$ defined by

$$g(z)=\left\langle \sum_{i,j} \delta(z-|z_{ij}|) \right\rangle l \Big/ [N(N-1)], \tag{17}$$

$$C_\mu(z)=\left\langle \sum_{i,j} (\mu_i\cdot\hat{\mathbf{z}})(\mu_j\cdot\hat{\mathbf{z}})\delta(z-|z_{ij}|) \right\rangle \Big/ \left\langle \mu^2 \sum_{i,j} \delta(z-|z_{ij}|) \right\rangle, \tag{18}$$

where μ_i is the dipole moment of the ith water molecule, $\hat{\mathbf{z}}$ is a unit vector along the cylinder axis, l is the length of the periodically repeated unit, and z_{ij} is the difference in z coordinates of the molecules i and j. These functions are identical (within the noise limits) for runs with 20 water molecules in a 3 Å channel with periodic boundaries 21.2 Å apart and for a run of 40 water molecules in a channel of twice the repeat length. They decayed to their limiting values by 10 Å. All other static and dynamic quantities are identical within the accuracy of measurement. We are confident that a 20 Å channel is sufficiently long to model the behavior of water in infinite channels of radius 3 Å and above. In channels that are narrow enough for the water molecules to lie in single file, chains of oriented water molecules may persist for long times and distances.

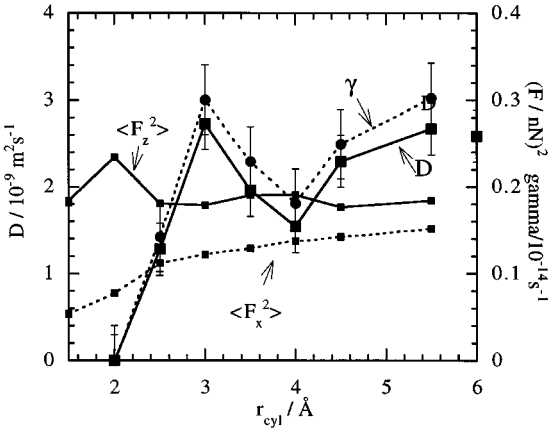

FIG. 4. Dynamics of water in channels of different radii. D (the left-hand scale) is the diffusion coefficient along the axis of the cylinder. D is related to the $\langle F_z^2 \rangle$ (the right-hand scale; units of nN^2; accuracy 3%) and to the rate γ (the right-hand scale: units of 100 ps^{-1}). $\langle F_x^2 \rangle$ is the corresponding mean square force in the x direction.

B. Dynamics in channels with water

Figure 4 shows the diffusion constant D for axial motion and the mean square forces in both the axial direction $\langle F_z^2 \rangle$ and the perpendicular direction $\langle F_x^2 \rangle$ together with the rate γ defined in Eq. (13). It is only in the narrowest channels where the water molecules are in single file that the diffusion is too slow to measure. In this case the whole column of water would have to move together for diffusion to occur. For channels with a radius of 3 Å and above the diffusion constant is the same order of magnitude as in the bulk liquid, but there are small variations, e.g., the structural stability of the channel with radius $r_{cyl}=4.0$ Å is reflected in a slowing of the dynamics. These results are all based on channels of about 20 Å in length. A run of water in the 3 Å channel at the same density but twice the length gave an indistinguishable plot of the mean square displacement as a function of time as well as the same structural and thermodynamic properties within the errors.

As mentioned in Sec. II, the rate of diffusion depends on the mean square fluctuation in the force and a quantity γ with dimensions of a rate; in the limit of Brownian motion the latter rate is just the inverse of the correlation time of the random forces acting on the diffusing molecule. The values of the mean square forces and γ measured for these systems show that the former vary rather little with cylinder radius so that the variation in the diffusion coefficient with r_{cyl} is due mainly to changes in the dynamics of the network as reflected in γ. The actual values of the rate γ correspond to time scales of femtoseconds. The molecules in the stable network ($r_{cyl}=4$) do not move so easily as in the less stable networks.

IV. SOLUTIONS OF SODIUM IONS IN CHANNELS

In this section we compare results for a specific ion (Na^+) as a function of channel radius.

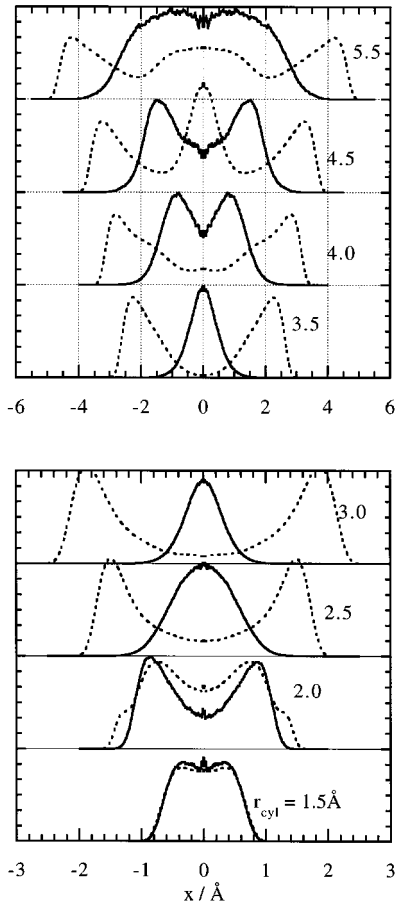

FIG. 5. Density profiles of Na^+ (solid line) and water (O atoms–the dotted line) across channels of different radii.

A. Structural features

Figure 5 shows the density distribution functions for the sodium ion (continuous lines) and the water molecules (water oxygen—dashed lines) projected along the channel length for a series of channels of different widths. The numbers of water molecules and channel lengths are given in Table II. There was no observable difference in this function for channels with a 3 Å radius and lengths of 21.2, 42.4, and 84.8 Å.

TABLE II. Simulations of Na^+ solutions (the numbers for pure water simulations are the same except that the solute was replaced by a water molecule).

Radius of channel r_{cyl}/Å	Length of channel l/Å	Number of waters	Number of solutes	Volume/molecule V/Å^3
2.0	28.6	11	1	29.94
2.5	30.5	19	1	29.94
3.0	21.2	19	1	29.97
3.5	19.5	24	1	30.01
4.0	19.1	31	1	30.00
4.5	19.3	41	1	29.95
5.5	18.9	59	1	30.44
3.0	42.4	39	1	29.97
3.0	84.8	79	1	29.97

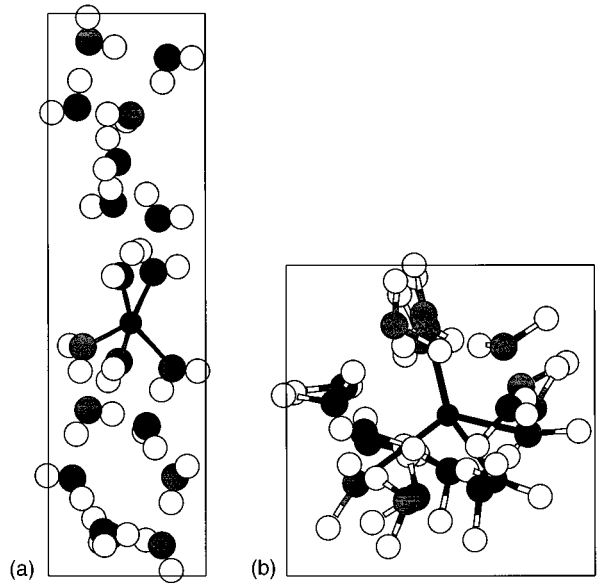

FIG. 6. Two views of a configuration from the simulation of Na^+ in a channel with radius 3 Å. (a) View of the molecular dynamics box from the side; the axis of the channel is vertical. (b) View down the axis of the channel. In this view the channel wall is a circle inscribed in the square shown.

We note that the sodium ion tends to avoid the outside of the channel which is preferentially occupied by water molecules (except in the narrowest channels). The only example where there is a significant distortion of the water structure compared with the pure water results shown in Fig. 2 is for the 4 Å radius channel. Examining individual configurations one finds that in the narrower channels (i.e., up to and including that with a radius of 3.0 Å) the water molecules in the ion's solvation shell lie above and below the ion. Figure 6 illustrates this; it shows two views of a configuration from the simulation of the 3 Å channel. At the instant at which this snapshot was taken the solvation shell is made up of two molecules above and three below the ion. Animations show that from time to time water molecules pass the ion, moving from below to above or vice versa. The average coordination number in this channel was 5.4. Figure 7 shows the coordination numbers as a function of radius. As the radius of the channel increases, the number of neighboring water molecules changes from 2 (with the molecules in single file) in the narrowest channel to about 6 in the widest channel. The coordination number found in simulations with the same potential in bulk is 5.9.[30] In the wider channels the overall orientation of the solvation shell is less affected by the channel geometry than in the example shown in Fig. 6. However it is only in the widest channel that the radial density of sodium ions in the interior of the channel becomes even approximately uniform (see Fig. 5). The observed positions of the sodium ions are the ones which allow the ion to maximize its bonding to the water. The changes in the solvation energy shown in Fig. 7 mirror the changes in the coordination number but remain higher than the value in simulations of bulk solution[30] (-745 kJ mol^{-1}).

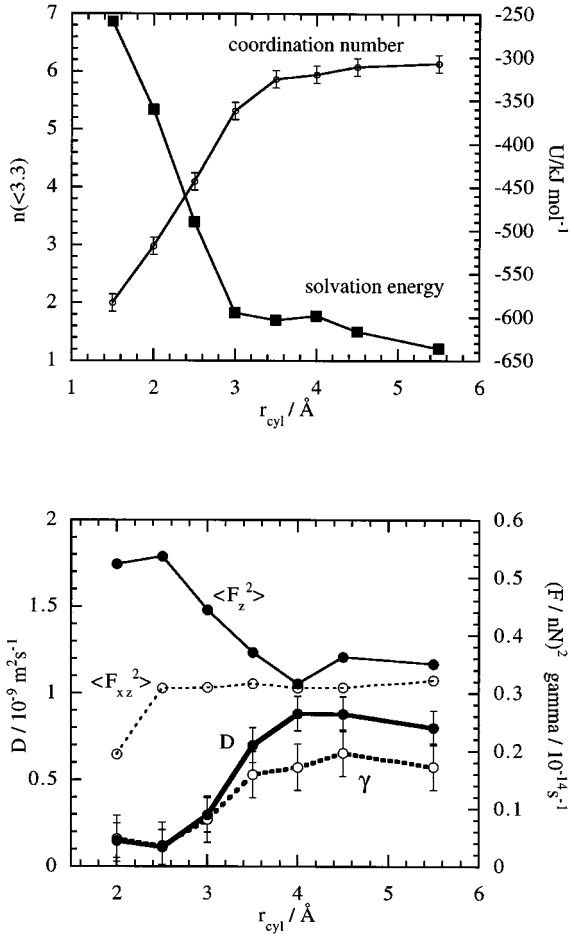

FIG. 7. Properties of Na^+ as a function of channel radius. Upper graph: Solvation energy (the right-hand scale; accuracy 1 kJ/mol) and coordination number (the left-hand scale). Lower graph: dynamics of sodium Na^+ ion. D (the left-hand scale) is the diffusion coefficient along the axis of the cylinder. D is related to the $\langle F_z^2 \rangle$ (the right-hand scale; units of nN^2; accuracy 3%) and to the rate γ (the right-hand scale: units of 100 ps^{-1}). $\langle F_x^2 \rangle$ is the corresponding mean square force in the x direction.

It will be recalled that in the 4.0 Å channel the structure with pure water was particularly stable. By contrast in this channel the structure around the sodium ion is less stable than the trend would suggest. In Fig. 7 we see that the solvation energy is less negative than expected and the solvation number is also possibly smaller than the trend would suggest. Further, the water structure is significantly distorted by the ions. This is the only channel for which one can readily see the consequences of the competition between the preferred water structure and the solvation structure around the ion.

Internal pressure and surface tension can be calculated in the same way as for the channels containing water and values are given in Table III. By comparison with Fig. 3 we see that there is little difference between the results for pure water and for the solution of sodium ions in channels whose radius is larger than 2.5 Å. This is not too surprising as both quantities are primarily due to the water molecules. In smaller channels the separation into surface tension and internal pressure components has no physical meaning. The value of

TABLE III. Pressures and enegies for Na^+ solutions in various channels. The pressures are reproducible to within 1 MPa.

Radius of channel r_{cyl}/Å	P_{zz} /MPa	P_{rad} /MPa	P_{int} /MPa	Surface tension /J m^{-2}
1.5	5.7	666	1326	0.0099
2.0	−67	724	1514	0.0158
2.5	251	705	1160	0.0114
3.0	109	564	1019	0.0137
3.5	153	457	761	0.0106
4.0	233	474	715	0.0096
4.5	183	461	740	0.0125
5.5	217	416	615	0.0109

P_{zz} is negative for Na^+ solutions in the 2 Å radius channel although the pure water has a positive value and the radial pressures are similar in the two cases.

The effects of concentration were investigated by comparing the results for the 3 Å channel with one ion, the same molecular density, and three different lengths, i.e., three different concentrations. The presence of an ion tends to align the water molecules with their dipole moments pointing away from the ion. This alignment is propagated in both directions along the channel axis until the point halfway between the ion and its image where there is no net alignment. It is this indirect interaction of the solvation shells which can give a concentration dependence to some quantities. We constructed the ion–axial dipole correlation function

$$C_\mu(z)=\left\langle \sum_i (\hat{\mu}_i\cdot\hat{z}_{Ii})\,\delta(z-|z_{Ii}|)\right\rangle \Big/ \left\langle \sum_i \delta(z-|z_{Ii}|)\right\rangle, \tag{19}$$

where z_{Ii} is the difference in z coordinates of the ion and molecule i and circumflexes denote unit vectors. We compared this function and the ion–water axial density distribution function for four systems, namely one Na+ ion in 3 Å cylinders of length 21.2, 42.4, and 84.8 Å, and in a 4.5 Å cylinder of length 19.4 Å. The axial distribution functions for the three 3 Å cylinders were indistinguishable. The ion–dipole correlation functions for the 42.4 and 84.8 Å channels are very similar to each other, but that for the 21.2 Å channel differs at distances greater than 5 Å. At distances less than 5 Å the alignment is high with $C_\mu(z)$ reaching values of 0.8. At $z=10$ Å where the shortest channel has no alignment, the value of $C_\mu(z)$ is 0.3 in the two longer 42.4 and 84.8 channels. This increased alignment changes the solvation energy from −594 kJ/mol (21.2 Å) to −604 kJ/mol (42.4 Å) and −597 kJ/mol (84.8 Å), respectively, and affects the dynamics. In the 4.5 Å channel the alignment is lower by 50% and we do not anticipate significant changes in the solvation energy or diffusion constants in these wider channels.

B. Diffusion

In bulk SPC/E water[30] the diffusion constant for sodium ions is 1.2×10^{-9} m^2 s^{-1} while that of water is 2.6×10^{-9} m^2 s^{-1}. One can explain this in part by the larger size of the sodium ion plus its hydration shell, and it is therefore not surprising that the diffusion of the sodium ions is more affected by confinement in a channel than is the diffusion of water. Figure 7 shows the solute diffusion constants and related quantities as a function of radius. The diffusion constant decreases as the channels get narrower.

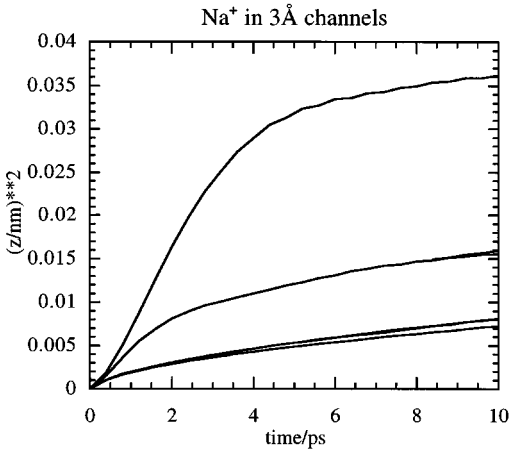

FIG. 8. Mean square axial displacement of the sodium ion in 3—AA channels of different lengths. Lower curves: three runs with length 21.2 Å; middle curves: two runs with length 42.4 Å; upper curve: a single run with length of 84.8 Å. Note that although the slopes at long times and hence the diffusion constants are very similar, the short time behavior varies considerably with channel length.

Changing the ion concentration has two effects, first the diffusion constant (as determined from the limiting slope of the mean square displacement) may be altered and second, the short time behavior is changed. This is shown for six runs in Fig. 8. Each of these runs was 5 ns long, and the mean square displacements calculated for 6000 time origins. The lowest lines are for the 21.4 Å channel, the middle ones for the 42.4 Å channel, and the top one for the longest channel (84.8 Å). The limiting slopes and diffusion constants do not change much [values of the diffusion constant are (in units of 10^{-9} m^{+2} s^{-1}) 0.30, 0.26, and 0.24 for the three runs at 21.2 Å; 0.19, 0.16 for the two runs at 24.2 Å, and 0.27 for the run at 84.8 Å]. The short time behavior is dramatically different. In the longest channel the limiting slope is not reached until 10–15 ps and the intercept of the asymptotic line on the $\langle z^2\rangle$ axis is much larger. The intercept may be interpreted as the square of the ion displacement due to the local motion before true diffusive motion sets in, e.g., in a solid the mean square displacement reaches a constant value asymptotically so in this case the intercept is equal to the square of the amplitude of the atom's vibrational motion within the crystal. The unexpected dependence of the intercept on the channel length indicates that as the channel gets longer there is a larger amplitude of local motion of the ion relative to the bulk water before diffusion sets in. The root mean square displacement as measured by the intercept ranges from 0.5 Å in the 21.2 Å length channel to 1.7 Å in the 84.8 Å length channel. This change may be the result of the larger density fluctuations due to the possibility of longer wavelength sound waves in longer channels.

Analyzing these results for diffusion in different channel

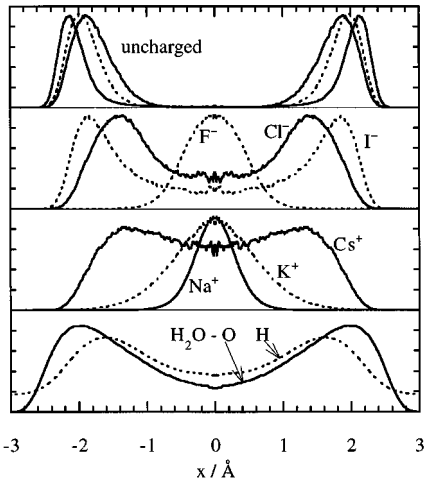

FIG. 9. Density profiles of solutes in a 3 Å channel. From bottom to top: water (H and O atoms); positive ions (Na^+, K^+, Cs^+); negative ions (F^-, Cl^-, I^-); uncharged species with radii corresponding to Na^+ (inner), K^+, Cs^+ (outermost).

widths into the product of a contribution from the mean square force and a rate constant for the force fluctuations γ, one finds that, unlike the pure water case, the changes in D are due to both an increase in the mean square force in the longitudinal direction as the channel gets narrower and a decrease in the rate γ. The mean square force is unaffected by concentration; the observed decrease in D with increasing box length is due to a change in the solvation dynamics.

V. VARIATION WITH ION RADIUS AND CHARGE

In this section we discuss the properties of a range of solutes in a particular channel, namely the one with 3 Å radius. We examine the effects of charge and size of solute, taking advantage of the freedom one has in a simulation of changing these properties independently. By doing this we can isolate the effects of charge and size and compare the extremes of hydrophilic and hydrophobic solvation by turning the charges on and off.

A. Structure and free energy

Figure 9 shows the axial projection of the density distribution functions for various solutes in the channel with a radius of 3 Å. These results are for one ion and 19 water molecules in a channel with a radius of 3 Å and length of 21.2 Å which are indistinguishable from the density distribution functions for one ion and 39 water molecules in a channel with twice the length. From top to bottom the graphs are for uncharged species, negative ions, positive ions, and pure water, respectively. There is a remarkable difference between the uncharged species and the ions and there are clear trends among the ions depending on their size. Uncharged species hug the outside of the cylinder, and have a maximum in their probability density near that of the water oxygen atoms. They avoid the center of the cylinder completely. There is only a small change in distribution with atomic radius. The ions, on the other hand, show a strong size dependence which is roughly the same for positive and negative ions. Smaller ions tend to lie in the center of the cylinder, while the larger ions are more likely to be found nearer the outside of the channel. Except for I^-, which has penetrated the water layer near the outside of the channel, the ions still lie nearer the channel axis than the water.

One can understand why ions might prefer to be in the center of the cylinder as in that position the ion is best placed to form as complete a solvation shell as possible from waters all around it. As can be seen from the configuration in Fig. 6(a), the Na^+ ion in the 3 Å channel forms a solvation shell with water molecules above and below in the axial direction. It is less clear at first sight why the larger ions should favor the outside of the channel. Even if a solvation shell fits less easily around a larger ion confined in a channel one would expect that a central position would be a better arrangement than for the ion to be situated in the solvation layer of the wall, and indeed our free energy calculations show this to be true as far as the ion–solvent energy interactions go. The solute and solvent interactions with the wall in our model are identical and purely repulsive—see Eq. (1). The reason that the large ions move to the wall is that entropic terms in the free energy become important.

In order to understand these results we performed Landau (or constrained) free energy calculations for I^-, Na^+, and hypothetical positive, negative, and neutral species with the same Lennard-Jones diameters as these two species, using the method described in Sec. II. Figure 10 shows the Landau free energy, $A(R)$, as a function of the distance, R, of the solute from the axis of the cylinder for the three small and three large solutes in these calculations. As $A(R)$ and $-TS(R)$ can only be determined to within an arbitrary constant, we have displaced the curves for convenience. The minima in $A(R)$ correspond to the most favorable position for the ion, which occur at the channel center for small ions and nearer the outside for larger ions and neutral species.

We now analyze the source of this varying behavior. As described in Sec. II, the Landau free energy can be written as the sum of five terms:

$$A(R) = -TS_{\mathrm{W}}(R) + U_{\mathrm{WW}}(R) + U_{\mathrm{SW}}(R) - U_{W\ \mathrm{wall}}(R) - TS_{\mathrm{S}}(R), \tag{20}$$

where the subscripts S and W refer to solute and water, respectively. The last contribution arises from the factor $2\pi R$ in the available volume as a function of R, giving

$$-TS_{\mathrm{S}}(R) = -kT\ \log(R/\text{Å}) + \text{const}, \tag{21}$$

which disfavors the center and is the cause of the rise in $A(R)$ very close to the center; otherwise it is a small effect. The variation of the rest of the entropy, S_{W}, is due to changes in the solute–water and water–water interactions. The more tightly bound the solvation shell the more its entropy is decreased, but at the same time the resulting modification of the water network may give an increase in entropy. We are unable to separate these effects in our calculations. The lower graph in Fig. 10 shows the entropic contribution to the free energy, $-TS_{\mathrm{W}}(R)$, plotted on the

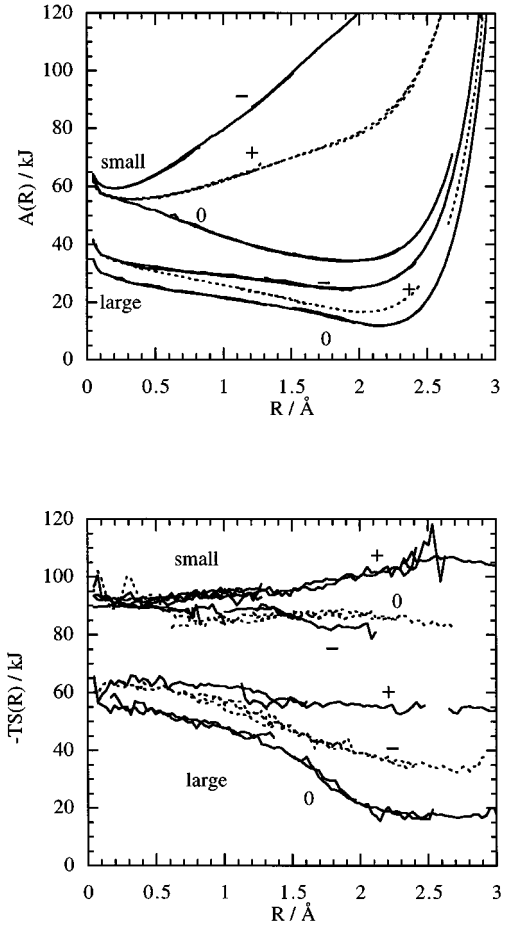

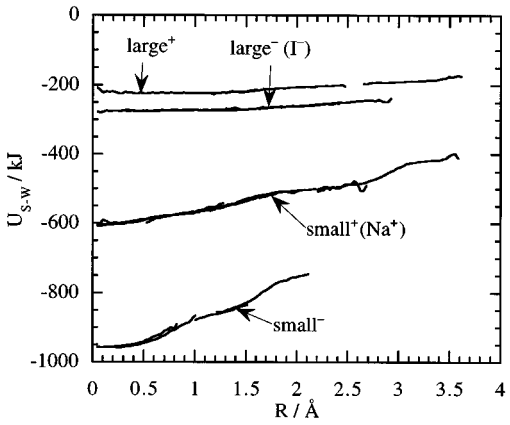

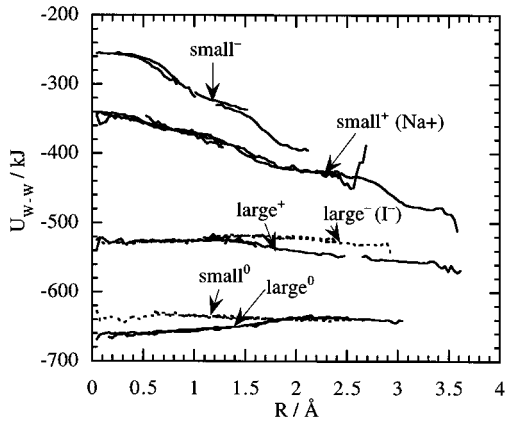

FIG. 10. Thermodynamics as a function of solute position relative to the axis of the channel. Upper graph: Landau free energies of small and large ions. Lower graph: corresponding entropic contributions $[-TS(R)]$. See Eqs. (14)–(16) for details and note that as both these functions contain an undetermined constant the vertical position of all these curves is arbitrary.

FIG. 11. Contributions to the potential energy as a function of solute position. Upper graph: Solute–water interaction energy; lower graph: water–water interaction. Unlike the quantities shown in Fig. 9 these energies are determined absolutely. The limiting values are in Table IV.

same scale as the free energy changes. Note that each curve can only be determined to an arbitrary constant, so the absolute values are meaningless; it is the trends that concern us. We see that the entropic contributions are not very important for the small solutes—that is, those with the same radius as Na^+. The entropy is a maximum at the center of the channel for the positive ion.

For the large solutes—that is those with the same radius as I^-—the entropic contribution is much more important and favors the outside of the channel. These solutes can be classified as structure making in the environment of the channel center so that the entropy of the water is increased as they are removed from the channel. This result for the confined ion is the opposite to the observed behavior in bulk, where I^- is found to be a structure breaker.[46–49]

Figure 11 shows the most important of the energetic terms, that is the solute–water potential energy (above) and the water–water potential energy (below). The solute–water interaction is straightforward to understand. It is stronger and hence more negative for small ions compared with large ones and is also stronger for negatively charged ions than for positive ions. This reflects the stronger interactions in the more compact solvation shell around small ions and the fact that the positively charged hydrogens can be approached more closely by negative ions than the oxygen by positive ions. The variation with ion position, which is what is important for the structure within the channel, always favors the center of the channel, and is larger for small ions than large ions. The solute–water interaction and its variation with ion position is negligible for the uncharged species.

The water–water potential energy $U_{WW}(R)$ which is shown in the lower part of Fig. 11 shows the extent of the disruption of the hydrogen-bond network by the solute. The limiting values for the solutes at the center of the cylinder are shown in Table IV. The differences between the values for 19 water molecules plus a solute molecule and those for 19 or 20 water molecules alone (given at the bottom of Table IV) provide a measure of the disruption of the hydrogen-bond network of the water by a solute in the center of the cylinder. As expected, the stronger the solvation of a charged species, the greater the disruption of the network. It is, however, the variation of the water–water energy with position R of the solute which contributes towards the preferred solute

TABLE IV. Water–water potential energy with solute on the cylinder axis. Δ_{19} and Δ_{20} are the differences in energy between the system with 19 water molecules and one solute molecule and one with no solute and 19 or 20 water molecules, respectively.

Charge	σ_{SO}/Å	Ion	$U_{WW}(0)$/kJ	Δ_{20}	Δ_{19}
−1	4.168	I^-	−530±3	117	81
+1	4.168		−523±5	124	88
0	4.168		−663±5	−16	−52
−1	2.876		−258±5	389	353
+1	2.876	Na^+	−340±10	307	271
0	2.876		−605±5	4	40

position. For small ions and the positively charged large ion U_{WW} falls with R, favoring the outside. There is little variation in U_{WW} for I^-, but it does have a weak maximum around $R=1.7$ Å. The entropic term shown in Fig. 10 favors the outside of the channel at least for large species. Thus for charged species we can say that small ions favor the channel center because the energetic terms dominate the Landau free energy, and large ions favor the outside as for them entropic terms dominate.

The neutral molecules behave somewhat differently. The small neutral solute seems to have remarkably little effect on either quantity suggesting that it has very little effect on the water hydrogen bonding. A detailed analysis of the various contributions shows that the large fall observed in Landau free energy toward the outside of the channel is made up of approximately equal contributions from small falls in the water–water, water–wall, and water–solute energies. The large neutral solute, a typical hydrophobic particle, is particularly interesting as it stabilizes the hydrogen-bonding network. This is shown by the fact that the values of Δ_{19} and Δ_{20} (see Table IV), the differences between U_{WW} for the system with a solute molecule and 19 waters, and for the system with no solute and 19 or 20 waters, respectively, is negative. There is also a large increase in entropy as the solute is pulled away from the center of the channel. This may be an example of ''iceberg'' formation which has long been postulated.[46,47] This enhanced ordering of water has also been been inferred from simulations of bulk solutions of methane in water.[50]

To sum up, the three important terms that determine $A(R)$ and hence the position of the solute in the channel, are the solute–water energy, the water–water energy, and the entropic term $-TS(R)$. The solute–water energy always favor the central position, but the other two terms tend to favor the outside of the channel. The behavior of small ions is dominated by their large solvation energy, while the behavior of larger ions and uncharged species is dominated by the entropic term due to the changes in water structure around the ion.

As we observed a concentration dependence of the diffusion constants for sodium ions in the 3 Å channel we carried out at 5 ns runs for all the charged species in cylinders of radius of 3 Å and two lengths, 21.2 and 42.4 Å. A comparison of such runs for one of the uncharged solutes (K) showed no differences in dynamics or statics, so runs for the other uncharged solutes were not repeated for longer channels. The radial density distribution functions were independent of channel length within the accuracy for which they could be determined. There is lowering of the solvation energy by 1%–3% for positive ions and 3%–4% for negative ions (the solvation energy is reproducible to an accuracy of about 0.2%). The mean square forces on the ions are independent of channel length to within their reproducibility. The axial ion–dipole correlation functions described previously were similar in magnitude for $z>12$ Å for all singly charged ions.

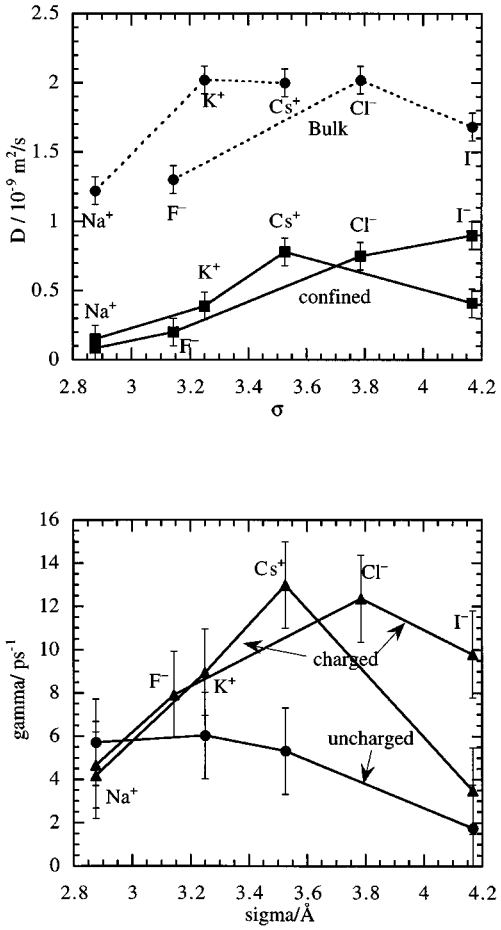

FIG. 12. Dynamics of solutes in the 3 Å channel as a function of ion size (Lennard-Jones ion–water parameter σ). Upper graph: Diffusion coefficients of ions in bulk and in the channel. Lower graph: The rate γ [defined in Eq. (13)] for charged and neutral species in the channel.

B. Diffusion and dynamics

One of the characteristic features of ion diffusion in bulk water that is observed both experimentally and in simulations is that the diffusion constants of positive ions rises to a maximum at Rb^+ as the ion radius is increased.[30] A similar phenomenon occurs with negative ions, but at a slightly larger radius at Br^-.[30,51] Figure 12 and Table V show our results for the 3.0 Å channel. In the upper graph the diffusion constants in the confined system are compared with those previously observed in simulations with the same potential in

TABLE V. Mean square forces and diffusion constants for solutes in 3 Å channels. Solutes marked with an asterisk are hypothetical entities the same size as the ion shown. The mean square forces are determined to 5% while the errors in the diffusion constants are comparable for the two channels.

Ion length	$\langle F_z^2\rangle$/nN^2	$\langle F_z^2\rangle$/nN^2	$D/10^9$ m^2 s^{-1} 21.2 Å	$D/10^9$ m^2 s^{-1} 42.4 Å
		Positive ions		
Na^+	0.44	0.31	0.32	0.19±0.07
K^+	0.35	0.18	0.46	0.39±0.07
Cs^+	0.26	0.12	0.83	0.78±0.07
$(I^*)^+$	0.12	0.08	0.75	0.41±0.1
Ca^{2+}	0.90	0.84	0.021	0.025±0.02
		Negative ions		
$(Na^*)^-$	00.91	0.99	0.060	0.085±0.04
F^-	0.61	0.48	0.28	0.20±0.1
Cl^-	0.26	0.16	0.97	0.75±0.1
I^-	0.17	0.10	0.63	0.90±0.1
		Neutrals		
(Na*)	0.016	0.031	5.8	
(K*)	0.017	0.040	5.6	5.4±0.1
(Cs*)	0.019	0.045	4.5	
(I*)	0.024	0.052	1.2	

a bulk system. We have included values for positive and negative ions with radii equal to those for I^- and Na^+, respectively. In the channel the diffusion constants of all the ions are considerably less than in an unconfined environment. The reduction in diffusion constant is approximately constant so that while Na^+, K^+, and F^- diffuse at about one-quarter of the rate they would have if they were unconfined, the larger ions are less affected, the rates being 40% of the bulk rate for Cs^+, 57% for Cl^-, and 37% for I^-. There are still maxima in the mobility versus ion radius curves for the positive ions but they appear to be shifted to larger ion radii. The diffusion constants for uncharged species on the other hand (see Table V) are much larger and decrease monotonically. Animations of our simulations in wider channels also reveal ions and water molecules overtaking each other during their diffusive motion along the channel length.

The effect of increasing the channel length (i.e., diluting the ions) is first to lower the diffusion coefficients with the exception of I^- (the values are given in Table V). Second, at short times the mean square displacements increase and the onset of the asymptotic behavior is delayed. The latter effect, which may be due to the local motion of the ion in its solvation cage or to density fluctuations in the channel, is more pronounced for the smaller ions. Its presence means that the average mean square displacement must be followed for long times to obtain reliable values for the diffusion constant. Our results are based on 80 ps length functions.

Using the analysis described in Eq. (13) we can use the measured force fluctuations to define a rate γ which is related to the time scale of fluctuations in the network in the channels. This quantity is shown in the lower part of Fig. 12. The first thing to note is that unlike the diffusion constants which differ by an order of magnitude, the values of γ for charged and uncharged species are comparable. The main reason that uncharged species diffuse more rapidly is that the random forces acting on them are smaller as they interact less strongly with their surroundings.

VI. CONCLUSIONS

In this work we have found that aqueous solutions in nanopores have a markedly nonuniform density with a layer of water molecules lining the walls of the channel. This suggests that the treatment of ion and water diffusion by continuum models[52] is unlikely to be valid for channels with radii smaller than 5–6 Å.[30,53] In a recent paper[21] Sansom *et al.* have simulated modified TIP3P water in cylindrical channels similar to ours, but of finite length with open ends. They studied channels with radii 3, 6, 9, and 12 Å, together with hourglass-shaped pores. They also see the formation of solvent layers. The main difference seems to be that they see a greater effect of confinement of the diffusion of the water molecules.

For channels containing pure water, molecular diffusion is only slowed significantly when the channel is narrow enough (radius 2 Å) that the molecules form a single file (see Fig. 4). In slightly larger channels we see a specific dependence of many properties on the channel size. In particular one channel, radius 4 Å, seems to be particularly stable energetically and has a decreased diffusion rate. Interestingly this is due to more nonlinear O–H contacts (Fig. 3) than one might expect from the general trend rather than an increased number of hydrogen bonds.

Sodium and calcium ions favor the regions with low water density (e.g., the centers of the smaller channels) and are always further from the channel walls than the layer of water molecules which line the channel. The rate of diffusion of sodium ions are slowed as a result of this confinement even in the wider channels studied here. This is due both to changes in the mean squared force $\langle F_z^2\rangle$ and in the rate γ.

Other solutes behave rather differently. Larger ions and uncharged species tend to favor the outer regions of the channel, and a Landau free energy analysis shows that, broadly speaking, this change is due to an increasing importance of the entropy for the larger ions. The preferred position of smaller and more highly charged ions at the center of the channel is the result of the dominance of the solvation energy over both the entropic terms and the water–water energy. The diffusion constants of these species in a particular small channel (3 Å radius) are reduced by an approximately constant amount from the corresponding values in bulk water so that more slowly moving ions have a larger percentage reduction. There is still a maximum in the diffusion-ion size relation as in bulk solutions, but, for positive ions, it is displaced to larger ion sizes.

The preference of uncharged species for the outside of the cylinder where they are in contact with the hydrophobic wall can be considered as a typical of hydrophobic interaction. The usual argument for the preference of hydrophobic species to aggregate is that this reduces the area of contact between the hydrophobic and hydrophilic molecules. The aggregation of small hydrocarbons is found to increase with

temperature, suggesting that the driving force is primarily entropic. However in other circumstances there is evidence for an enthalpic contribution as the hydrogen bonding in the solvation shell is sometimes stronger than in bulk water. Here we find that the driving force for the large uncharged species to go to the wall is entropic and that, when isolated in the center of the channel there is an energetic stabilization of the hydration shell.

Our simulations of ions in smooth channels provide no information about their entry into the channel but only information about their subsequent motion within it after admission. As observed earlier, a uniform distribution of dipoles on the walls of a smooth perfectly cylindrical channel produces no radial field and has no effect on the disposition of the ions in the channel (e.g., whether it is off-center or near the wall) or on their diffusive motion along it in an infinitely long channel, but it could change the chemical potential of ions within the channel to selectively prevent or ease their entry. For instance, a uniform distribution of dipoles on the channel wall with the negative ends pointing toward the channel axis could discourage the entry of anions as observed in gramicidin. Distortions in the shape of the channel or a nonuniform distribution of dipoles on the channel surface could produce a field (radial and axial) and influence the positions and rates of passage of ions along the channel.

These simulations of ion structure and mobility in smooth channels of different radii provide a useful reference against which real systems such as nanopores, zeolites, and biological channels can be judged. Our results for the mobilities of ions in smooth channels with radii ranging from 2 and 5.5 Å are rather different from observations of ion transport in the dimer of gramicidin A which has been studied in detail.[1] In this channel, hydrogen-bonded carbonyl groups line a pore of radius 2 Å and length close to 26 Å with walls made up of two right-handed beta helices with mainly hydrophobic amino acid side chains extending into the cell membrane. Permeation in this channel involves collective single file translation of partially dehydrated ion and water molecules through a narrow pore of a width which is at the lower limit of our simulations. The channel is permeable only to water and cations; it is impermeable to anions and is blocked by divalent cations such as Ca^{2+}. Also it has been observed in simulations[1,4] that Cs^{+} lies closer to the center of the gramicidin channel, and Na^{+} lies off the axis. This is the reverse of what is observed in our simulations of structureless and smooth channels that are slightly wider (radius 3 Å). We attribute this difference to the narrower channel width and to specific molecular interactions between binding sites and carbonyl groups on the gramicidin wall and the water molecules and ions.

ACKNOWLEDGMENTS

We would like to thank Dr. S. H. Lee for the use of his program which provided the basis of the program used here; the Queen's University of Belfast and EPSRC (Grant No. GR/K20651) for computational equipment and the Queen's University for visitor's funds. We thank the referee for pointing out the importance of dipole alignment along the channel axis.

[1] B. Roux and K. Karplus, Annu. Rev. Biophys. Biomol. Struct. **23**, 731 (1994).
[2] B. Roux, in *Computer Modelling in Molecular Biology*, edited by J. Goodfellow (VCH, Wenhem, 1995).
[3] B. Hille, *Ionic Channels of Excitable Membranes* (Sinauer, Sunderland, MA, 1992).
[4] P. C. Jordan, J. Phys. Chem. **91**, 6582 (1987).
[5] P. C. Jordan, Biophys. J. **58**, 1133 (1990).
[6] P. C. Jordan, 1988, in *Transport through Membranes: Carriers, Channels and Pumps*, edited by A. Pullman (Kluwer, Dordretch, 1988).
[7] V. Dorman, M. B. Partenskii, and P. C. Jordan, Biophys. J. **70**, 121 (1996).
[8] A. Pullman, Chem. Rev. **91**, 793 (1991).
[9] P. P. Schmidt, Adv. Quantum Chem. **25**, 47 (1992).
[10] J. Kasianowicz and S. M. Bezrukov, Biophys. J. **69**, 94 (1995).
[11] S. M. Bezrukov and J. Kasianowicz, Phys. Rev. Lett. **70**, 2352 (1993).
[12] D. H. J. McKay, P. H. Berens, K. R. Wilson, and A. J. Hagler, Biophys. J. **46**, 229 (1984).
[13] K. Cooper, E. Jakobsen, and P. Wolynes, Prog. Biophys. Mol. Biol. **46**, 51 (1985).
[14] S. W. Chiu, S. Subramanian, E. Jakobsson, and J. A. McCammon, Biophys. J. **56**, 253 (1989).
[15] S. W. Chiu, J. A. Novotny, and E. Jakobsson, Biophys. J. **64**, 98 (1993).
[16] J. Aquist and A. Warshel, Biophys. J. **56**, 171 (1989).
[17] D. Nicholson, J. Chem. Soc. Faraday Trans. **92**, 1 (1996).
[18] S. Murad, P. Ravi, and J. G. Powles, J. Chem. Phys. **98**, 9771 (1993).
[19] B. K. Peterson, K. E. Gubbins, and F. van Swol, J. Chem. Phys. **93**, 679 (1990).
[20] S.-H. Suh, S.-B. Rho, and S.-C. Kim, J. Chem. Eng. Jpn. **26**, 431 (1993).
[21] M. S. P. Sansom, I. D. Kerr, J. Breed, and R. Sankararamakrishnan, Biophys. J. **70**, 693 (1996).
[22] J. Breed, R. Sankararamakrishnan, I. D. Kerr, and M. S. P. Sansom, Biophys. J. **70**, 1643 (1996).
[23] H. J. C. Berendsen, J. R. Grigera, and T. P. Straatsma, J. Phys. Chem. **91**, 6269 (1987).
[24] L. X. Dang, J. Chem. Phys. **96**, 6970 (1992).
[25] L. X. Dang, Chem. Phys. Lett. **227**, 211 (1994).
[26] D. E. Smith, L. X. Dang, and B. C. Garrett, J. Chem. Phys. **99**, 2972 (1993).
[27] L. X. Dang and P. A. Kollman, J. Phys. Chem. **99**, 55 (1995).
[28] L. X. Dang, J. Chem. Phys. **96**, 6970 (1992).
[29] L. X. Dang, J. Am. Chem. Soc. **117**, 6954 (1995).
[30] S. H. Lee and J. C. Rasaiah, J. Phys. Chem. **100**, 1420 (1996).
[31] M. Ferrario, M. L. Klein, and I. R. McDonald, Mol. Phys. **86**, 923 (1995).
[32] M. P. Allen and D. J. Tildesley, *The Computer Simulation of Liquids* (Clarendon, Oxford, 1987).
[33] D. A. McQuarrie, *Statistical Mechanics* (Harper and Row, New York, 1976).
[34] G. M. Torrie and J. P. Valleau, J. Comput. Phys. **23**, 187 (1977).
[35] J. S. van Duijneveldt and D. Frenkel, J. Chem. Phys. **96**, 4655 (1992).
[36] R. M. Lynden-Bell, J. S. van Duijneveldt, and D. Frenkel, Mol. Phys. **80**, 801 (1993).
[37] R. M. Lynden-Bell and D. J. Wales, J. Chem. Phys. **101**, 1460 (1994).
[38] S. H. Lee, J. C. Rasaiah, and J. Hubbard, J. Chem. Phys. **86**, 2383 (1987).
[39] M. Gerstein and R. M. Lynden-Bell, J. Mol. Biol. **230**, 641 (1993).
[40] J. N. Israelachvili and G. E. Adams, J. Chem. Soc. Faraday Trans. I **74**, 975 (1978).
[41] S. J. O'Shea, M. E. Welland, and T. Rayment, Appl. Phys. Lett. **60**, 2356 (1992).
[42] S. Okazaki, K. Nakanishi, H. Touhara, and Y. Adachi, J. Chem. Phys. **71**, 2421 (1979).
[43] S. Okazaki, K. Nakanishi, H. Touhara, N. Watanabe, and Y. Adachi, J. Chem. Phys. **74**, 5863 (1981).
[44] A. Wallqvist and B. Berne, J. Phys. Chem. **99**, 2885 (1995).
[45] P.-L. Chau, T. R. Forester, and W. Smith, Mol. Phys. (in press).
[46] H. S. Frank and M. W. Evans, J. Chem. Phys. **13**, 507 (1945).
[47] H. S. Frank and W.-Y. Wen, Faraday Discuss. Chem. Soc. **24**, 133 (1957).

[48] R. W. Gurney, *Ionic Processes in Solution* (Dover, New York, 1963).
[49] F. Franks, *Water* (The Chemical Society, London, 1983).
[50] C. H. Bridgeman, A. D. Buckingham, and N. T. Skipper, Chem. Phys. Lett. **253**, 209 (1996).
[51] H. S. Frank, in *Chemical Physics of Ionic Solutions*, edited by B. E. Conway and R. G. Barradas (Wiley, New York, 1956).
[52] A. E. Hill, Cytology **163**, 1 (1995).
[53] J. Hubbard and P. Wolynes, in *The Chemical Physics of Ion Solvation Part C*, edited by R. R. Dogonadze, E. Kalman, A. A. Kornyshev, and J. Ulstrup (Elsevier, New York, 1985).